Mechanisms of Methanol Decomposition on Platinum: A Combined Experimental and ab Initio Approach

D. Cao, G.-Q. Lu, and A. Wieckowski*

Department of Chemistry, University of Illinois at Urbana-Champaign, Urbana, Illinois 61801

S. A. Wasileski and M. Neurock*

Department of Chemical Engineering, University of Virginia, Charlottesville, Virginia 22904

Received: January 7, 2005; In Final Form: March 9, 2005

The dual path mechanism for methanol decomposition on well-defined low Miller index platinum single crystal planes, Pt(111), Pt(110), and Pt(100), was studied using a combination of chronoamperometry, fast scan cyclic voltammetry, and theoretical methods. The main focus was on the electrode potential range when the adsorbed intermediate, CO_{ad}, is stable. At such "CO stability" potentials, the decomposition proceeds through a pure dehydrogenation reaction, and the dual path mechanism is then independent of the electrode-substrate surface structure. However, the threshold potential where the decomposition of methanol proceeds via parallel pathways, forming other than CO_{ad} products, depends on the surface structure. This is rationalized theoretically. To gain insights into the controlling surface chemistry, density functional theory calculations for the energy of dehydrogenation were used to approximate the potential-dependent methanol dehydrogenation pathways over aqueous-solvated platinum interfaces.

1. Introduction

The electrocatalytic decomposition of methanol over platinum in acidic media has been studied in great detail,[1−7] yet the elementary paths are still not understood. Several surface-adsorbed intermediates and bulk products have been identified, including CO_{ad} which is the main stable surface product, other less-stable surface intermediates such as $HCOO_{ad}$,[7] with CO_2 being the primary solution-phase product,[1,5] and other minor solution-phase products such as formaldehyde and formic acid.[8−17] A multi-path mechanism shown in Scheme 1 has been proposed to account for the data available in the literature.[1,5,10,18−22] While some of the surface species are still hypothetical or even controversial (e.g., $HCHO_{ad}$ or $HCOH_{ad}$), the scheme provides a realistic portrait of the complex overall pathways involved in methanol oxidation on Pt. This scheme is simplified somewhat in the electrode potential range where CO_{ad} is stable on the Pt electrode surface, as path 2 (among others) is missing as will be described shortly. This electrode potential range is very interesting and of clear relevance to the chemistry involved in direct methanol fuel cells (DMFC). The work presented herein focuses on the chemistry occurring within this potential range, specifically elucidating the "dual path" of methanol oxidation. The term "dual path" encompasses two primary reactivity routes: one leading to stable CO_{ad} and its oxidation (if relevant) and another to soluble product species that are not obtained by the oxidation of stable CO_{ad}. At higher potentials, where CO is no longer stable on the surface, the dual path also refers to two reaction routes: one passing through the CO_{ad} intermediate and a second through other reactive intermediates.

More recently, surface-enhanced infrared studies of the methanol oxidation reaction and the dual path mechanism carried out by Osawa and co-workers[7] identified surface formate as a reactive intermediate upon methanol oxidation on a polycrystalline platinum electrode at $E > 0.5$ V vs RHE (where RHE refers to the potential of the reversible hydrogen electrode; i.e., the potential of the $2H^+ + 2e^- \leftrightarrow H_2$ reaction). Stuve and co-workers[20−22] observed CO_2 production on both Pt(100) and Pt(111) at potentials where adsorbed CO is surface stable, indicating CO_2 was formed via the parallel non-CO pathway. They also found that the parallel path accounted for more than 75% of the total CO_2 produced at 0.6 V. Formaldehyde and formic acid have been detected as the soluble products of methanol electrooxidation on polycrystalline platinum and Pt(111).[8−10] The amount of formaldehyde can be quite significant.[10] In preliminary investigations, we found that, at short reaction times (<1.5 s), the dual path mechanism is applicable for some platinum single-crystal surfaces.[19] We also confirmed that the dual path occurs over a polycrystalline platinum electrode.[18]

SCHEME 1[a]

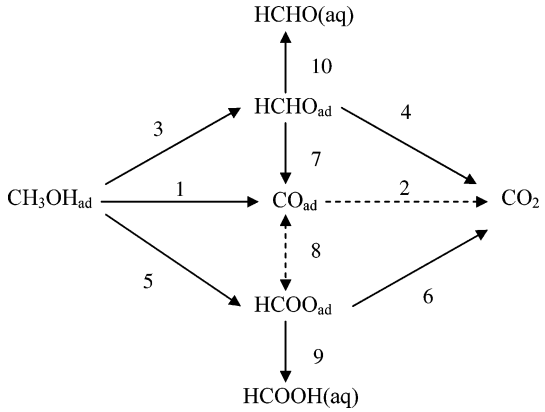

[a] A schematic representation of the pathways for methanol oxidation on platinum electrodes. It is assumed that CO_{ad} is not oxidized in the potential range from 0.2 to 0.45 V, which is denoted by the broken line 2.

* Corresponding author. E-mail: andrzej@scs.uiuc.edu.

10.1021/jp0501188 CCC: $30.25
Published on Web 05/19/2005

As discussed in ref 18, we define a parameter $r = Q_{CA}/Q_{CV}$, where Q_{CA} is the methanol oxidation charge obtained from chronoamperometry and Q_{CV} is the charge associated to the oxidation of CO_{ad} (formed from methanol decomposition) obtained from fast scan cyclic voltammetry. In the electrode potential range where adsorbed CO is stable on the electrode surface, all of the CO generated by the decomposition of methanol remained on the electrode surface. Therefore, if methanol oxidation proceeds through the sole CO-pathway ($CH_3OH \rightarrow CO + 4H^+ + 4e^-$), then $r = 2$. If, on the other hand, $r > 2$, a dual-path mechanism is occurring[18] because Q_{CA} includes not only the charge generated in the CO-pathway, but also the charge produced in the non-CO pathway, for example, the formation of soluble formaldehyde. As r becomes larger, the non-CO pathway becomes more important. Reported herein is chronoamperometry/fast-scan cyclic voltammetry results at long adsorption times for the three low-index faces of platinum single-crystal electrodes, completing the project originated in ref 19, in which surface structure effects on dual-path mechanism were studied for a very short reaction time (1.5 s). In this study, we find the dual path mechanism is platinum surface structure independent. However, the threshold potential where the decomposition of methanol proceeds via parallel pathways, forming products other than CO_{ad}, depends on the electrode surface structure. To begin to establish insight into this behavior, ab initio quantum-chemical calculations of the methanol dehydrogenation pathways over Pt(111) under relevant electrochemical conditions were carried out.

2. Experimental Methods

Chronoamperometry (CA) and cyclic voltammetry (CV) measurements were carried out in two 2-compartment electrochemical cells each equipped with a built-in Luggin capillary.[23] The first cell, referred to herein as cell-**A**, contained 0.1 M H_2SO_4 and was used for single-crystal quality checks and background measurements. The second cell, cell-**B**, contained 0.1 M H_2SO_4 + 0.1 M CH_3OH and was used for measurements of methanol decomposition (combined CA and fast scan CV). The working electrodes were three platinum single crystals [Pt(111), Pt(110), and Pt(100)], ca. 0.3 cm in diameter. Prior to each measurement, the platinum single-crystal electrode was annealed in the hydrogen/air flame, cooled in a hydrogen/argon stream, and immersed in ultrapure water that has been deaerated by bubbling hydrogen/argon gas.[24,25] The electrode was then transferred, under the protection of a droplet of deoxygenated water, into cell-**A**. The quality of the surfaces was checked by cyclic voltammetry at 0.05 V/s using a meniscus configuration. Figure 1 shows typical CV curves for Pt(111), Pt(110), and Pt(100). The actual surface areas were determined using hydrogen adsorption−desorption charges.[24] After an appropriate single-crystal surface was obtained (as indicated by CV), background measurements were carried out. The single-crystal electrode was then transferred into cell-**B** under the protection of a droplet of 0.1 M H_2SO_4. A series of programmed potential steps, CA, and the fast-scan CV sweeps[18] were carried out; see below (Section 4.1).

The counter electrode was a platinum wire immersed in the main electrode compartment. The reference consisted of a Ag/AgCl/NaCl (3.0 M) electrode connected via Luggin capillary, completely isolated from the working electrode area. However, all potentials in this paper are reported versus RHE.

The 0.1 M H_2SO_4 (SFG, double distilled from Vycor) and 0.1 M CH_3OH (Fischer Scientific, Optima) solutions were prepared using ultrapure water (Millipore Milli-Q, 18.2 MΩ cm^{-1}, 4 ppb total organic carbon). The solutions were deoxygenated by bubbling argon (Matheson Tri-Gas, research purity, 99.9999%, O_2 < 0.5 ppm) for 2 h in the cells prior to use and were protected under argon during the measurements. Hydrogen and argon used for single-crystal annealing are of ultrahigh purity (99.999%) from Matheson Tri-Gas.

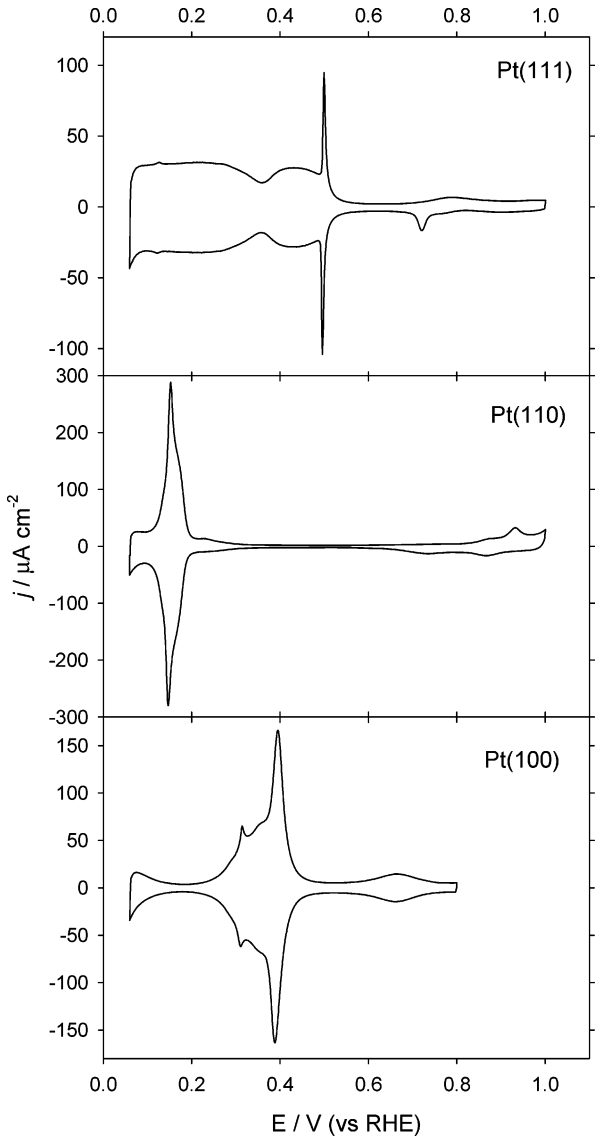

Figure 1. Cyclic voltammograms of Pt(111), Pt(110), and Pt(100) in 0.1 M H_2SO_4. The scan rate is 50 mV/s.

All measurements were carried out at room temperature (25 ± 2 °C) using a computer-controlled potentiostat (Eco Chemie, autolab PGSTAT100 with GPES software). The *iR*-drop was compensated by using the positive feedback function of the potentiostat. The data analysis was performed using the GPES software. Error bars are standard errors showing that the data are reported on the confidence level of 68%. From 3 to 5 measurements were taken for a single data point.

3. Computational Methods

Generalized gradient-corrected periodic DFT calculations were carried out to determine the reaction energies for methanol decomposition over model Pt(111) surfaces in aqueous media as a function of electrochemical potential. The Pt(111) surface was modeled using a three-layer periodic slab oriented in a face-centered cubic (fcc) lattice arrangement with 27 Pt atoms per

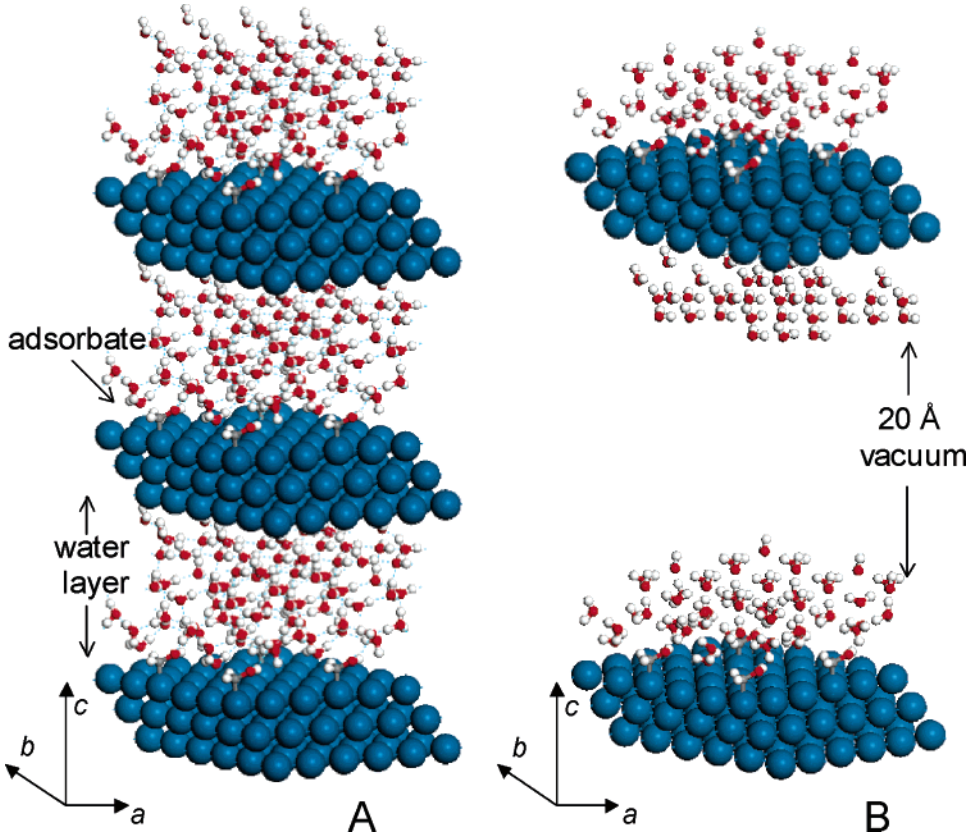

Figure 2. (A) Graphical representation of the aqueous-phase periodic-slab configuration, with the lattice vectors *a*, *b*, and *c* labeled, depicting 1/9 coverage CH_2OH over Pt(111) in a (3 × 3) surface structure. (B) Corresponding representation of the unit-cell configuration where a layer of vacuum is inserted in the aqueous layer to generate an internal vacuum reference.

unit cell repeating in a p(3 × 3) surface structure. The interatomic distances of the center Pt layer were held fixed at the bulk-phase value (2.775 Å), while all other metal atoms were allowed to relax to their equilibrium positions. The optimal density of water was established by expanding the lattice vector perpendicular to the surface plane to determine the lowest energy Pt(111)-H_2O structure. For the unit cell with 24 H_2O molecules, the optimum density is 0.86 g/mL, similar to that for ice. One CH_xO species is adsorbed per unit cell at a surface coverage of 1/9 and is solvated by 23 water molecules completely filling the ∼13.5 Å spacing between Pt slabs, as depicted in Figure 2A. The methanol intermediates and water molecules are fully optimized to their equilibrium configuration.

The salient features of tuning the Pt(111) surface potential are briefly described here. A complete description of this method and its application is given in ref 26. The surface potential of the Pt slab is varied by adding or removing a specified number of electrons to the unit cell. The excess or depletion of charge is countered by a homogeneous background of opposite charge, which is distributed across the entire unit cell. The background charge combined with the polarizable water molecules simulates the electrochemical double layer, thus generating an electric field at the solution−slab interface.[26] An important aspect of this method is the ability to estimate the surface potential of the slab with no external charge and estimate the corresponding surface potential shift when electrons are added or subtracted from the system. Estimating the surface potential of the former case is discussed first.

The surface potential is determined from the energy at the fermi level (i.e., the energy per electron in the highest filled electronic state) referenced to a known system potential within the calculation, in this case, vacuum. The internal vacuum reference is generated by creating a new unit cell with a 20 Å layer of vacuum[27] inserted in the aqueous layer of the fully optimized system at zero external charge ($q = 0$), as depicted in Figure 2B. The potential of the vacuum layer at the position bisecting the upper and lower slab surfaces is set to equal 0 V versus vacuum by adding a constant ($\Delta\phi$). The fermi level output is correspondingly adjusted by $\Delta\phi$ to produce the fermi energy versus vacuum (i.e., the surface potential vs vacuum). This internally referenced surface potential is converted to the scale of the normal hydrogen electrode (NHE) by subtracting 4.8 V (i.e., 0 V vs vacuum = −4.8 V vs NHE), although experimental estimates of the vacuum reference on the hydrogen scale are estimated to be between 4.4 and 4.8 V.[28,29] Similar surface−adsorbate energetics and surface potentials have been calculated with both three- and five-layer slabs for aqueous Ni(111) systems.[30] A more detailed analysis of the method indicates that the absolute estimated potential is only accurate to about ±0.5 V.[26] However, comparisons of similar systems using identical reference conditions produce relative potential differences that are typically accurate on the order of 0.1−0.2 V.

Variations in the surface potential, induced by externally charging the Pt(111) slab, can also be determined by defining an internal reference within the aqueous layer itself. In this case, the water molecules that reside along the center line within the aqueous layer are held fixed during the optimization of the $q \neq 0$ systems. (Note that the frozen water molecules do not directly hydrogen bond with the adsorbate and therefore do not affect the optimum structure of the CH_xO species.) The corresponding potential at the position of the fixed water molecules is shifted by a new $\Delta\phi$ to be equal to that for the same position of the $q = 0$ system, which was previously referenced versus vacuum.

The fermi energy is likewise shifted by $\Delta\phi$, generating a surface potential versus vacuum for the $q \neq 0$ systems and similarly converted to the hydrogen scale by subtracting 4.8 V (vide supra). The adsorbate structure, system energy, and surface potential for a variety of external charges (q) can be determined in this manner.

The surface−adsorbate interaction and hence the surface potential expectedly varies with the adsorbate species, resulting in variations in the potential at $q = 0$ (as well as at $q \neq 0$) for the different CH_xO species. To determine potential-dependent reaction energies for the individual methanol dehydrogenation steps, the energy for the reactant and product states must be compared at equivalent potentials (rather than at equivalent charges), which require an estimation of the surface potential. Potential-dependent reaction energies are determined by subtracting the best-fit curve of computed potential-dependent energies of the product state (i.e., $CH_{(x-1)}O + H_3O + 22H_2O + 27Pt$) from that of the reactant state (i.e., $CH_xO + 23H_2O + 27Pt$), thereby maintaining constant potential and equal numbers of atoms in both reactant and product states.

Previous experimental results carried out over Pt(111) indicate the likely presence of defect sites which may alter the kinetics.[31] To begin to understand the influence of defect sites, calculations were performed over the stepped Pt(211) surface for comparison with those over Pt(111). More specifically, the vapor-phase structures, binding energies, and reaction energies for the first dehydrogenation of methanol step were determined over stepped Pt(211) surface as well as Pt(111) surfaces. In both cases, a unit cell of 27 Pt atoms oriented in a three-layer fcc slab was utilized with the Pt−Pt bond distances of the center Pt layer held fixed at the bulk-phase (2.775 Å). The CH_3OH, CH_2OH, CH_3O, and H species were adsorbed in various binding sites on the surfaces to determine the most favorable configuration as discussed below.

All calculations were carried out using the Vienna Ab initio Simulation Package (VASP)[32] periodic density functional theory (DFT) code. The Kohn−Sham one-electron equations are solved in the DFT-GGA approximation using the RPBE functional[33,34] for the aqueous-phase systems and the PW91[35] functional for the vapor-phase system. The electron density is described using plane waves with a kinetic-energy cutoff of 396.0 eV, determined by oxygen. The ion cores are described using ultra-soft pseudopotentials[36] developed using the PW91[35] correlation and exchange approximations. It has been shown that the use of PW91 pseudopotentials available in VASP with the RPBE functional affects chemisorption energies by less than 0.03 eV.[37] The Brillouin zone is sampled using a grid of $3 \times 3 \times 1$ Monkhorst-Pack special k-points for all adsorbate structures.[38] Partial occupancies of the wave function are allowed by including order-two Methfessel-Paxton smearing[39] at a width of 0.2 eV.

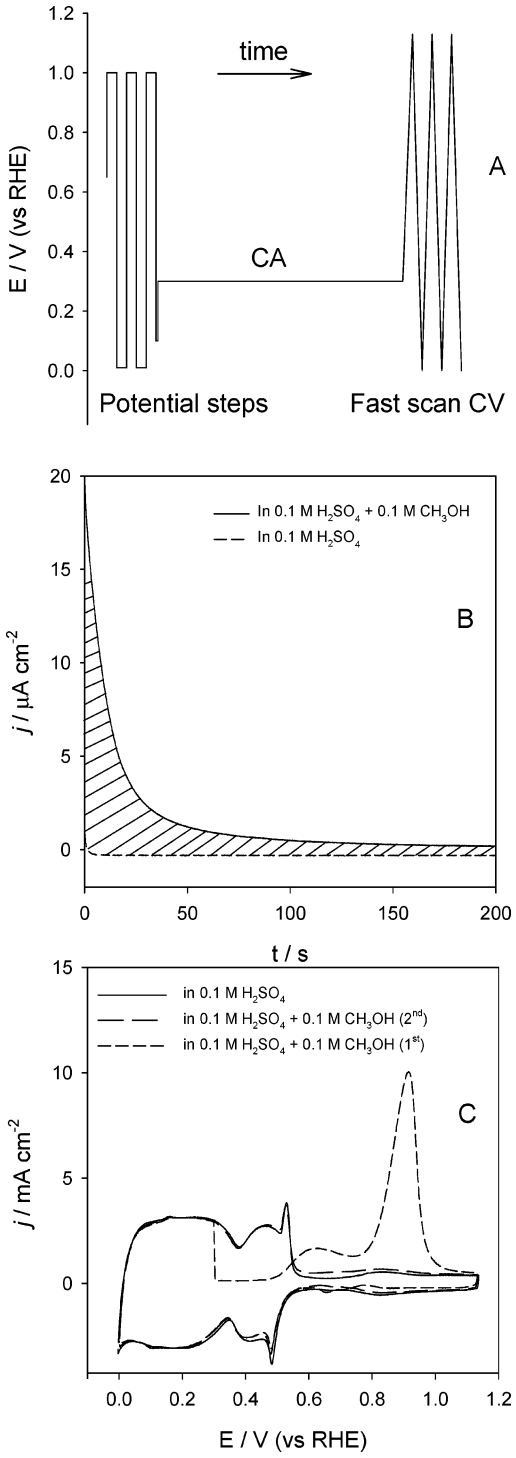

Figure 3. The combination of chronoamperometry and fast scan cyclic voltammetry. (A) Potential steps for cleaning, (B) chronoamperometry, (C) fast scan cyclic voltammetry.

4. Results and Discussion

4.1. Combination of Chronoamperometry and Fast Scan Cyclic Voltammetry. Figure 3 demonstrates a typical combined chronoamperometry and fast scan cyclic voltammetry experiment carried out over the Pt(111) surface in 0.1 M H_2SO_4 + 0.1 M CH_3OH. The experiment consists of (i) programmed potential steps for cleaning, (ii) the CA, and (iii) the fast scan CV performed one after the other without losing the potential control. The cleaning potential steps (Figure 3A) were applied between 1.0 V (oxidation) and 0.01 V (reduction) with the waiting time of 1s at each step. 1.0 V was selected as the upper limit potential, as any surface adsorbed species from methanol (i.e., CO_{ad}) were removed at this potential and no noticeable surface oxides were formed, so that the Pt(111) surface structure was not disordered. The lower limit potential was set at 0.01 V to fully reduce platinum surface oxides to restore the metallic surface, and to avoid hydrogen gas evolution. The last potential step was at 0.1 V for 0.2 s. In this way, good data reproducibility was obtained. Figure 3B (solid line) shows the chronoamperometric curve recorded at 0.3 V in 0.1 M H_2SO_4 + 0.1 M CH_3OH immediately following the cleaning step. The potential at which methanol decomposition was carried out is termed a measuring potential (E_M). The corresponding background curve was

recorded under the same conditions in 0.1 M H_2SO_4 (dash line). The total charge (Q_{CA}) involved in the methanol oxidation was obtained by integrating the background-corrected currents over the reaction time, as illustrated by the shade area in Figure 3B. The background correction eliminates possible contributions from oxygen reduction, hydrogen oxidation, anion desorption, and the double layer charging from the methanol oxidation charge measurements, leading to good accuracy in Q_{CA}. The value of Q_{CA} is the sum of charges generated in all of those steps of methanol oxidation possibly occurred at a specific measuring potential (E_M) and reaction time. According to Scheme 1, $Q_{CA} = \sum Q_i$ ($i = 1-9$, whenever appropriate).

Figure 3C shows the fast scan cyclic voltammograms (5 V/s), recorded immediately after the CA is terminated, with first and second scans shown as short and long dash lines, respectively. The scan started from the measuring potential, here $E_M = 0.3$ V, in the positive-going direction. The upper limit potential is set to 1.13 V, so that adsorbed CO is completely stripped while the Pt(111) surface structure is still not disordered. The lower limit potential is near 0 V, which just precedes the hydrogen evolution, so that the hydrogen adsorption/desorption peaks are fully developed. The fast scan CV in blank 0.1 M H_2SO_4 electrolyte solution without CH_3OH was also recorded under the same conditions and is included in Figure 3C (solid line). It can be seen that the second scan CV in 0.1 M H_2SO_4 + 0.1 M CH_3OH (long dash line) is nearly the same as the one recorded in 0.1 M H_2SO_4 (solid line). The modification to the hydrogen and bisulfate adsorption−desorption peaks by the presence of methanol is negligible, and the oxidation peak for CO_{ad} is absent. This result indicates that at sufficient high scan rates, Pt(111) is almost "blind" to the presence of methanol in the solution. The first positive-going scan recorded immediately after the CA (short dash line, Figure 3C) displays a peak at ca. 0.9 V. This peak is due to the oxidation of adsorbed CO accumulated during the decomposition of methanol. The charge corresponding to the oxidation of the CO_{ad} (Q_{CV}) was obtained by integrating this CO stripping peak, and subtracting the background contribution, which is associated with platinum surface oxidation and anion readsorption. The second and subsequent scans in 0.1 M H_2SO_4 + 0.1 M CH_3OH are identical, and they closely resemble the CV in 0.1 M H_2SO_4; therefore, the second scan was used for the background correction. The combination of chronoamperometry and fast scan cyclic voltammetry enables us to measure, with a good accuracy and low scatter, the total charge for the decomposition of methanol (Q_{CA}) and for the oxidation of CO_{ad} generated from methanol (Q_{CV}). Here,[18] the ratio of Q_{CA} to Q_{CV} (eq 1) is a convenient parameter for the study of the dual path.

$$r(E,t) = \frac{Q_{CA}(E,t)}{Q_{CV}(E,t)} \qquad (1)$$

When the measuring potential (E_M) is lower than the onset potential for CO_{ad} oxidation, the CO_{ad} formed during methanol decomposition is stable on the platinum surface. Under such conditions, if pathway 1 (complete methanol dehydrogenation, Scheme 1) is the only pathway for methanol decomposition, then $Q_{CA} = Q_1$, $Q_{CV} = Q_2$, and r is then equal to 2. If other pathways coexist together with pathway 1 (see Scheme 1), then r is larger than 2. Therefore the r-value indicates whether the dual path mechanism is operational (vs the pure dehydrogenation reaction). The salient assumption is that the CO is stable up to 0.45 V as shown, e.g., in Figure 5. In this work, the measuring potential E_M was between 0.2 and 0.5 V, and the reaction time

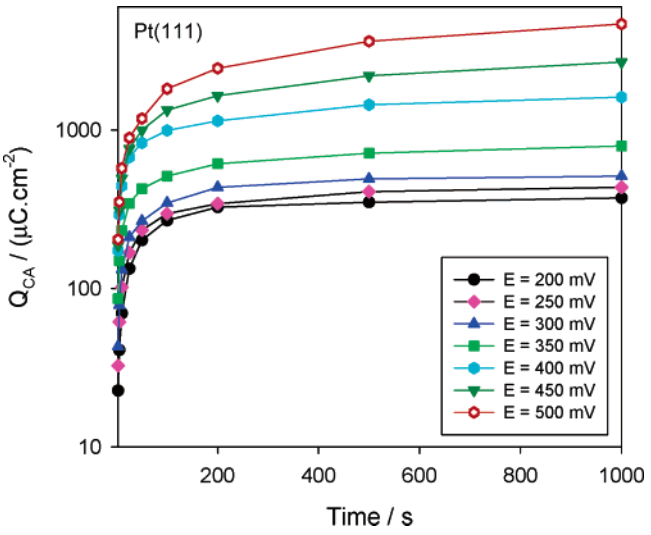

Figure 4. Plots of log Q_{CA} as a function of reaction time at the electrode potentials studied in 0.1 M H_2SO_4 + 0.1 M CH_3OH.

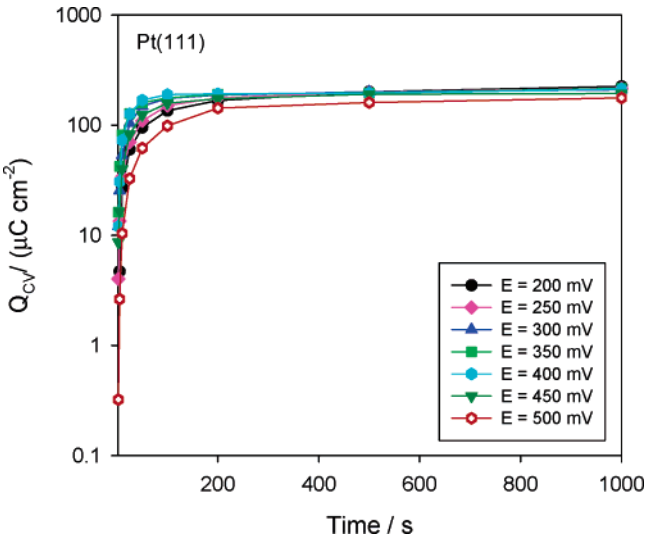

Figure 5. Plots of log Q_{CV} as a function of reaction time at the electrode potentials studied in 0.1 M H_2SO_4 + 0.1 M CH_3OH.

t was 500 and 1000 s. The long time range yields large changes for both chronoamperometry and cyclic voltammetry, and under such conditions the data are the most reliable.[40]

4.2. Q_{CA}, Q_{CV} (CO-Coverage), and "r" Data Analysis. As pointed out above, Q_{CA} is the total charge involved in the decomposition and oxidation of methanol. Figure 4 shows the plots of log Q_{CA} as a function of reaction time for Pt(111), and for all electrode potentials examined here. As expected, Q_{CA} increases with reaction time. In Figure 5, the CO striping charge (log Q_{CV}) is plotted as a function of reaction time for Pt(111). Similar trends were found for all of the platinum surfaces investigated. As mentioned above, only the data obtained at the highest adsorption times, where the Q_{CA} charge essentially stabilizes, will be analyzed further.

Figure 6 shows data of Q_{CV} (measured at 500 s) as a function of the electrode potential for all surfaces studied in this work. (Data at 1000 s show the same trends.) Obviously, Q_{CV} data are proportional to the CO coverage. Notice that between 0.2 and 0.4 V for Pt(111) and Pt(110), the CO coverage remains nearly constant, but drops slightly later. However, the CO coverage−electrode potential relationship for Pt(100) is different: the coverage increases up to 0.3 V, passes through a maximum, and then falls off. This phenomenon could not result

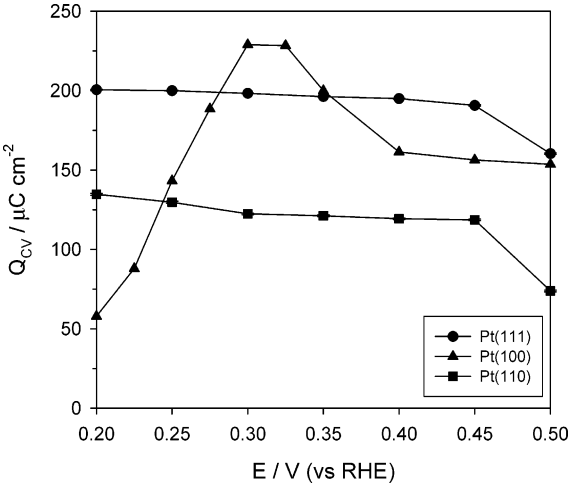

Figure 6. Plots of Q_{CV} (measured at 500 s) as a function of the electrode potential in 0.1 M H_2SO_4 + 0.1 M CH_3OH for Pt(111), Pt(100), and Pt(110). (Data at 1000 s show the same trends.)

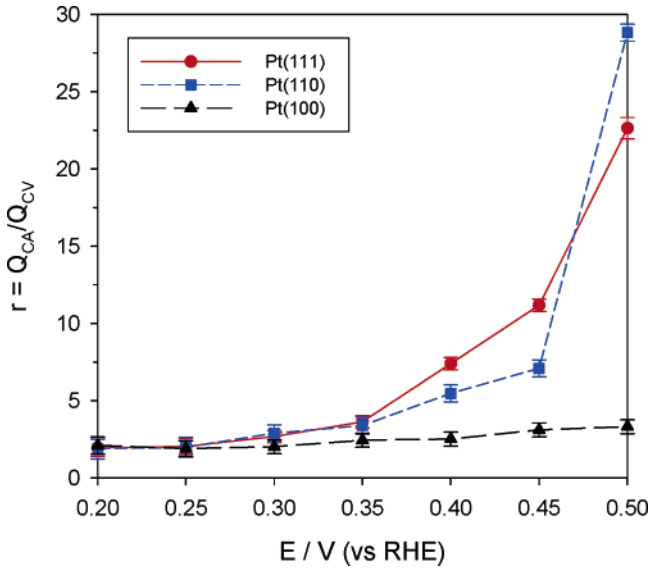

Figure 7. Plots of *r* (measured at 500 s) as a function of the electrode potential in 0.1 M H_2SO_4 + 0.1 M CH_3OH. (Data at 1000 s show the same trends.)

from CO_{ad} oxidation because CO_{ad} is stable on Pt(100) at potentials below 0.4 V.[14] The coadsorption of hydrogen and anions (in the appropriate potential ranges) may account for this finding.[41] This needs to be investigated further, and the data need to be cross-referenced to those obtained by other methods.

Figure 7 shows plots of the *r* ratio measured at 500 s as a function of the electrode potential. For Pt(100), the *r* ratio is around 2 over a broad potential range, showing no other pathway(s) than the decomposition of methanol to CO_{ad} on Pt(100). The *r* ratio measured on Pt(111) and Pt(110) is also around 2 but only at potentials below 0.35 V, indicating that up to this potential and for all surfaces studied, the sole reaction is methanol dehydrogenation to CO_{ad} (on the confidence level of 68%).

Data at higher potentials for Pt(111) and Pt(110) demonstrate the surface structure dependent dual path. The data between 0.35 and 0.45 V are the most meaningful because, at higher potentials, the surface states of Pt(111) and Pt(110) may be different. It is well known, for example, that Pt(110) is oxidized at lower potentials than Pt(111). Clearly, species other than CO_{ad} are formed more actively on Pt(111) than on Pt(110). This indicates that the pathways other than CO formation become effective above 0.35 and that the rate is higher for Pt(111) than for Pt(110). The secondary path is likely due to formaldehyde formation based on the previous analysis to the products of methanol oxidation. For example, by using HPLC, Iwasita and co-workers[10] found that 81% of the products were formaldehyde after 15 min electrolysis of methanol on Pt(111) at 0.6 V in 0.1 M CH_3OH and 0.5 M H_2SO_4. Korzeniewski and co-workers[9] reported 30% formaldehyde in a short (6 min) period of electrolysis of methanol on smooth polycrystalline Pt at around 0.4−0.5 V, as analyzed using a sensitive fluorescence assay. Baltruschat and co-workers[12] studied electrooxidation of methanol on nanoparticle Pt by DEMS and found that formaldehyde and formic acid were formed in a parallel pathway at high potential. The concentration of these soluble products depends on the concentration of methanol. All of these studies agreed on that dual-pathway mechanism is operational at high potential, and significant amounts of soluble products were generated by the parallel non-CO pathway, particularly on the smooth platinum surface because the soluble products are rapidly transported away from the electrode and their concentrations remain very low, so the readsorption and further oxidation is insignificant. Our results shows that, for Pt(111) and Pt(110), at potentials higher than 0.35 V, *r* is larger than 2 and increases rapidly with the increase of potential (Figure 7). This clearly indicates that a secondary path other than CO-path opened at higher potential, and the contribution of the secondary path is significant at high potential. This result is in good agreement with other studies, as discussed above. In addition, our study gives an approximate threshold potential for the secondary path and shows the surface structure dependence on the dual-path mechanism.

4.3. Ab Initio Results for Methanol Dehydrogenation over Pt(111). Density functional theory (DFT) calculations were carried out to help elucidate the specific elementary steps involved in the pathways for methanol dehydrogenation and to provide insight into the nature of the dual path for the chronoamperometry/cyclic voltammetry (CA/CV) results just described for model (111), (100), and (110) catalyst surfaces. To this end, we examine the full CH_3OH dehydrogenation pathway for the most stable low-index plane of platinum, Pt(111), to compare to the experimental results.

The theoretical investigations of methanol dehydrogenation over platinum surfaces presented in the literature thus far involve studies of vapor-phase (i.e., under ultrahigh vacuum conditions) homolytic C−H and O−H cleavage reactions using cluster[42,43] and periodic surface models[44−46] as well as aqueous-phase homolytic dehydrogenation using periodic models under static[47] and dynamic[48] conditions. Recently, we have presented the mechanism for the more energetically favorable heterolytic aqueous-phase dehydrogenation, but without consideration of the electrochemical potential.[49] The ab initio calculations presented herein are for heterolytic methanol dehydrogenation in an aqueous-phase under conditions where the surface potential is tuned to investigate potential regions relevant to experiment.

The DFT calculations model the aqueous-phase Pt(111)−adsorbate interactions by using a 1/9 coverage (i.e., 3 × 3 overlayer) of CH_xO intermediates fully solvated by explicit H_2O molecules, as depicted in Figure 2A. The structures of the surface Pt atoms, adsorbed CH_xO species, and aqueous layer are fully optimized so as to include changes in Pt(111)−CH_xO interactions due to hydrogen bonding between the adsorbed intermediate and the solution phase. The initial structure of the water network along with the optimal water density at the metal

surface were optimized previously.[49] The surface potential for each Pt−CH_xO system is varied by externally charging the metal surface.[26,50] A double-layer subsequently results due to the interaction of the excess surface charge and a corresponding counter charge distributed across the entire polarizable solvent layer. The resulting adsorbate structures are fully optimized at each charge to obtain the optimum system energy as a function of potential, with only the water molecules directly in the middle of the cell remaining fixed so as to provide a reference potential. A fairly wide potential region is investigated in this study so as to encompass the experimentally relevant conditions, necessary upon considering the ±0.5 V inaccuracy in the estimated potential for the zero-external charge system (vide supra).

Contributions from potential-induced water activation (i.e., formation of surface hydride or hydroxide toward more negative or more positive potentials, respectively) and other coadsorbed species (such as stable CO_{ad}) were not considered herein. The dehydrogenation chemistry is assumed in this analysis to be predominantly controlled by the surface potential, suggesting that perturbations of the local electronic structure by coadsorbed species (i.e., through-metal interactions) as well as steric repulsion due to lateral (i.e., through-space) interactions are small. However, such an assumption is only valid for low coadsorbate coverages, which may not be the case because CO_{ad} is quite stable. Coverage-dependent dehydrogenation energetics will be presented in the future but are beyond the scope of this preliminary study. Regardless, the influence of such coadsorbates on the calculated energies for methanol dehydrogenation is expected to be small.

For systems with potentials more positive than the zero-charged case, the lowest-energy dehydrogenation paths appear to be heterolytic, thus resulting in the formation of a solvated $H_3O^+_{(aq)}$ species along with an electron, which is donated to the metal surface. Corresponding homolytic dehydrogenation[47,48] for CH_3OH_{ad} to CH_3O_{ad} + H_{ad} over Pt(111) with no external charge results in a reaction energy that is 43 kJ/mol more endothermic that the heterolytic mechanism[49] (i.e., CH_3OH_{ad} to CH_3O_{ad} + $H_3O^+_{(aq)}$). Therefore, a heterolytic pathway is assumed to control the dehydrogenation energetics over the entire potential range considered (even at more negative potentials where the presence of surface hydride may be expected).

A consequence of the heterolytic dehydrogenation pathway is the formation of a solvated proton, which generates a discontinuity in the pH of the inner layer as the reaction proceeds. A similar discontinuity occurs in the calculation due to the limited size of the unit cell (CH_xO and 23 H_2O molecules) and the necessity for equal numbers of atoms in the product and reactant states (having hydronium ion concentrations of 0 and ~2 M, respectively). This unavoidable inconsistency in the unit-cell pH along with the unknown inner-layer pH hinders a direct comparison with the experimental bulk pH. If the experimental [H_3O^+] is assumed to be between 0.2 and 2 M for the 0.1 M H_2SO_4 conditions utilized here (reasonable because the inner-layer pH is expected to be lower due to the concentration gradient of the dehydrogenated protons at the metal interface), the calculated potential-dependent energy curves should be shifted between 0 and −0.08 V (determined via Nernst behavior of 0.06 V per pH unit), well within the error of the estimated potential. Therefore, the differences in pH between the experimental and computational systems are ignored. The optimized structures for the eight different adsorbed CH_xO species over Pt(111) are given in Figure 8a−h for the zero-external charge systems. In this study, we find that methanol is most favorably adsorbed atop on Pt(111) via the O atom (Figure 8a), which maintains favorable hydrogen bonding of the OH group with nearby water molecules, rather than via the CH_3 group as determined in previous aqueous-phase calculations of methanol adsorption.[48]

The corresponding system energies, E, calculated as a function of applied potential are plotted in Figure 9A, C, E, and G for the structures relevant to the first, second, third, and fourth consecutive heterolytic dehydrogenation steps, respectively. A closer analysis of Figure 9A reveals that the points indicated by black symbols at potentials between −0.8 and −0.5 V vs NHE are those corresponding to the three $q = 0$ systems. The potentials determined for all of the $q = 0$ systems are not equivalent because each has different Pt(111)−CH_xO interactions and therefore different surface charge densities. While the estimation of the potential may be in error by as much as ±0.5 V on an absolute scale, each system potential was calculated in a similar fashion such that each potential can be comparable to one another within 0.1−0.2 V (vide supra). To analyze the calculated reaction energies under electrochemical conditions (where the potential not the charge is the tunable parameter), the individual system energies must be compared at constant potential.

Plotted below each E versus potential plot in Figure 9 are the corresponding potential-dependent reaction energies, ΔE, in Figure 9B, D, F, and H, respectively. The dotted line represents $\Delta E = 0$ (i.e., where the dehydrogenation energetics are thermoneutral). For ease of comparison, all E versus potential and ΔE versus potential plots in Figure 9 are given on the same scale.

In the following analysis of the reaction mechanism, the preferred pathway is determined from the most favorable energies of dehydrogenation for each elementary step rather than from the more computationally intensive determination of the transition state energy. This analysis assumes the Bell−Evans−Polanyi principle to be true, where the reaction rate (determined from the energy of the transition state) scales with the thermodynamic reaction energy, which has been shown to be valid for homolytic vapor-phase dehydrogenation of methanol over Pt(111).[46] The following analysis, however, is qualitative only. A more quantitative analysis would require the simulation of actual activation barriers, which is currently being conducted.

Based on this assumption, our calculations show that a potential-induced conversion from a single to dual dehydrogenation path is likely and initiates at the first dehydrogenation step. As shown in Figure 9B, the reaction energy (ΔE) for C−H cleavage of adsorbed methanol (CH_3OH_{ad}) to form the hydroxymethyl (CH_2OH_{ad}) intermediate is more exothermic than corresponding O−H cleavage to form the methoxy (CH_3O_{ad}) intermediate at all potentials considered, indicating that the most-favorable dehydrogenation path occurs via the CH_2OH_{ad} intermediate similar to results of previous homogeneous aqueous-[47,48] and vapor-phase[44−46] dehydrogenation studies. However, upon close examination of Figure 9A, the curvature and slope of the energy versus potential curves for the CH_2OH_{ad} and CH_3O_{ad} species (□ and △, respectively) are quite different (the latter having a greater potential dependence) and appear to likely cross at higher potentials, indicating that under positive potential conditions the reaction energy for O−H cleavage is anticipated to become equally or perhaps more favorable than for C−H cleavage of methanol (Figure 9B). This indicates that the occurrence of a dual path is expected toward positive potentials, as determined from the CA/CV experiments at +0.35 V vs NHE for Pt(111) (vide supra), and that the two paths differ

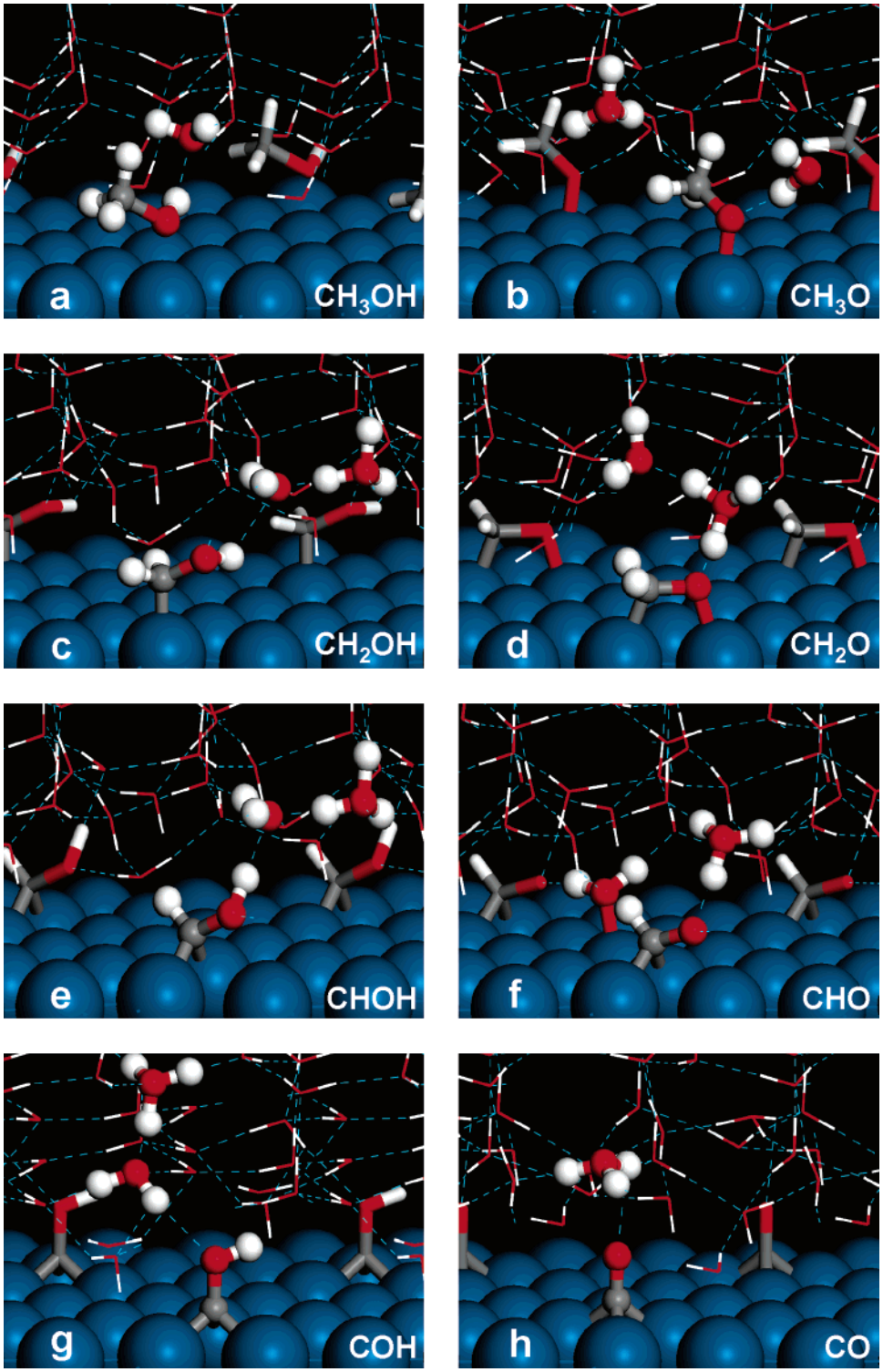

Figure 8. Optimized structures of CH_xO species, as indicated, over aqueous-solvated Pt(111) as determined by DFT.

by the initial C−H versus O−H cleavage steps. The reaction to form the methoxy intermediate may become more prevalent near defect sites as discussed below.

Subsequent dehydrogenation of the CH_2OH_{ad} and CH_3O_{ad} species indicates a continued partition of the mechanism into two distinct pathways. The CH_2OH_{ad} intermediate formed in step one (Figure 9B) further dehydrogenates via a second C−H bond activation step to form the adsorbed hydroxymethylene ($CHOH_{ad}$) intermediate as illustrated by the more-exothermic ΔE values in Figure 9D as compared to the endothermic activation of the O−H bond to form adsorbed formaldehyde (CH_2O_{ad}). In contrast, formaldehyde is formed via the exothermic activation of the C−H bond of CH_3O_{ad} (Figure 9D). These results suggest that the CH_2O_{ad} formed in the reaction proceeds via the CH_3O_{ad} intermediate, which is likely to be formed at more positive potentials. The subsequent desorption of CH_2O_{ad} into solution would result in a larger Q_{CA} value in the CA/CV experiments, and a measured r greater than 2.

Following the dehydrogenation path further, the produced CH_2O_{ad} that does not desorb from the surface [or oxidize to formic acid (HCOOH), for example] can undergo further highly exothermic C−H cleavage steps to form adsorbed formyl

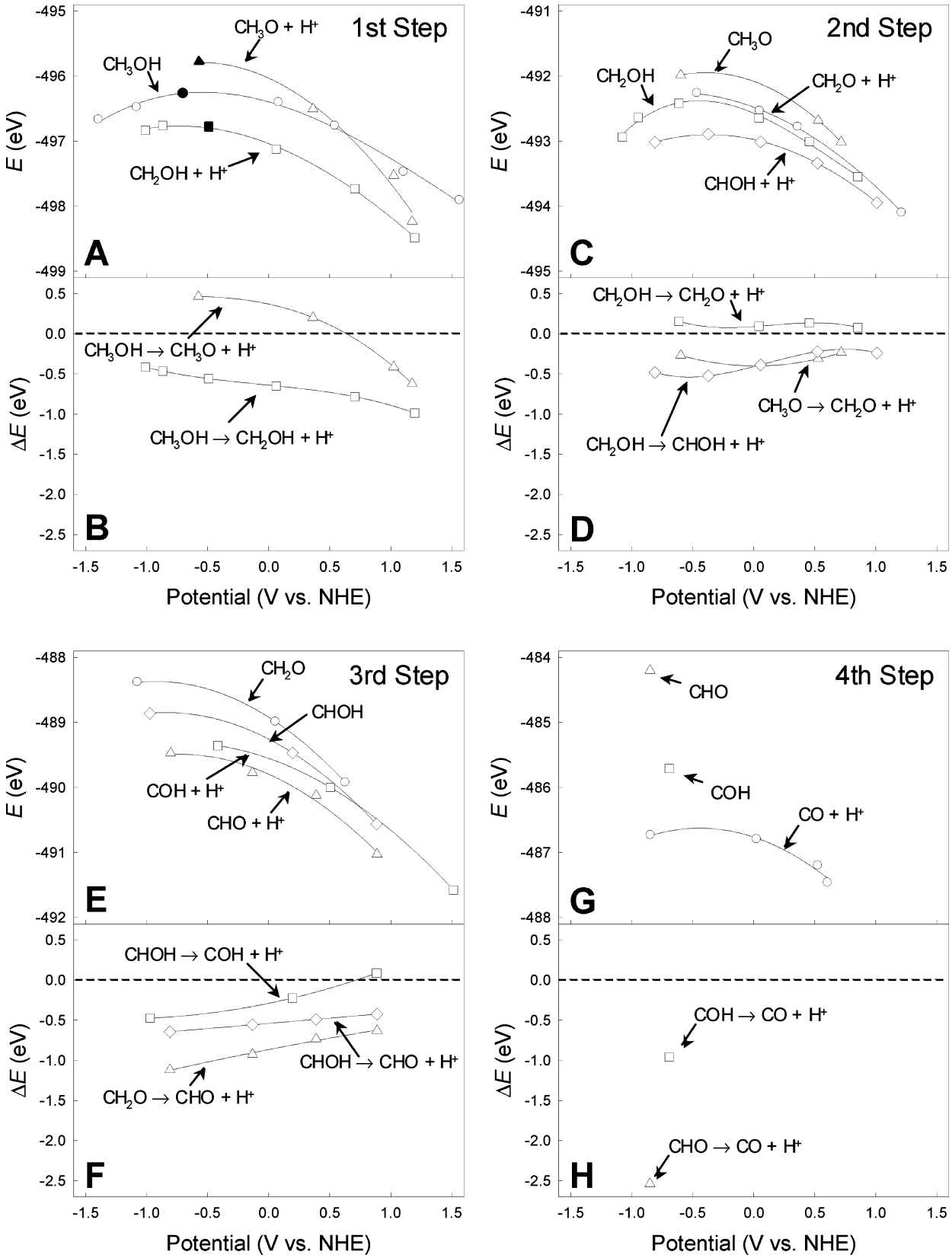

Figure 9. Potential-dependent system energy (upper plot) and reaction energy (lower plot) for the first, second, third, and fourth consecutive methanol dehydrogenation steps, as indicated, over Pt(111) as determined by DFT. Black symbols in Figure 9A refer to the systems at $q = 0$ (see text).

(CHO_{ad}) and carbon monoxide (CO_{ad}) species (Figure 9F and H, respectively). In addition, $CHOH_{ad}$ can react through either C−H or the more exothermic and therefore more likely O−H bond cleavage steps to form hydroxymethylyne (COH_{ad}) or CHO_{ad}, respectively (Figure 9F). In the fourth dehydrogenation step, conversion of both COH_{ad} and CHO_{ad} to form stable CO_{ad} is highly exothermic (Figure 9H) and energetics at only one system potential (i.e., that corresponding to $q = 0$) could be calculated because the reactant (COH_{ad} or CHO_{ad}) states optimized to the product ($CO_{ad} + H_{aq}$) state for $q > 0$ systems.

SCHEME 2: A Schematic Representation of the Specific Intermediates Involved in the Pathways for Methanol Dehydrogenation

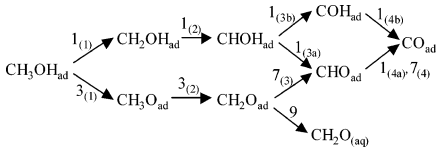

TABLE 1: Binding and Reaction Energies for CH_3OH, CH_2OH, CH_3O, and H over Pt(111) and Pt(211)

	Pt(111)	Pt(211)
	E_b	E_b
CH_3OH_{ad}	−0.36	−0.43
CH_2OH_{ad}	−2.14	−2.34
CH_3O_{ad}	−1.51	−2.25
H_{ad}	−2.84	−2.99
	ΔE	ΔE
$CH_3OH_{ad} \rightarrow CH_2OH_{ad} + \_H_{ad}$	−0.33	−0.60
$CH_3OH_{ad} \rightarrow CH_3O_{ad} + \_H_{ad}$	+0.64	−0.17

The specific elementary steps for methanol dehydrogenation from the proposed overall pathways depicted in Scheme 1 are elaborated further in Scheme 2. Overall, the dehydrogenation steps determined by DFT show the occurrence of a fully exothermic path to form CO_{ad} at potentials between −0.5 and +1 V vs NHE (path 1, Schemes 1,2). This path begins with an initial C−H cleavage of CH_3OH_{ad} to form CH_2OH_{ad} (step $1_{(1)}$, Scheme 2) and likely proceeds via steps $1_{(2)}$, $1_{(3a)}$, and $1_{(4a)}$. At potentials more positive of +0.5 V vs NHE, a second path, which leads to an initial O−H activation step to form CH_3O_{ad} (path 3, Schemes 1, 2), involving steps $3_{(1)}$ and $3_{(2)}$ to form CH_2O_{ad}, becomes exothermic and a possible reaction path. The reaction energy difference at +0.5 V vs NHE, however, is still nearly 0.7 eV less favorable for this path than the major methanol decomposition path to form hydroxymethyl. At potentials that approach +1.2 V vs NHE, the energy difference between this secondary path and that of the primary path becomes small enough to begin to account for the relative selectivity of the secondary path. The adsorbed CH_2O_{ad} can desorb in step 9 (Schemes 1, 2), producing an *r* value greater than 2 in the CA/CV charge analysis. Alternatively, CH_2O_{ad} can further dehydrogenate to form stable CO_{ad} via steps $7_{(3)}$ and $7_{(4)}$ (path 7, Schemes 1,2).

The results herein suggest that the secondary path becomes feasible at potentials on the order of +1.2 V vs NHE, which is still higher than that seen in the experiment. The potential at which the secondary path becomes energetically feasible with respect to the primary path can shift to lower potentials, however, if we consider the possibility that methanol is activated at coordinatively unsaturated step sites,[31] which are known to be present on Pt(111) single-crystal surfaces. As a means of simple comparison, we carried out calculations to examine the change in the binding energies and the overall reaction energies for the initial C−H and O−H cleavage steps for the vapor-phase methanol over a stepped Pt(211) surface along with those for the Pt(111) surface, which are listed in Table 1. The optimal structures and binding sites for CH_3OH_{ad}, CH_3O_{ad}, CH_2OH_{ad}, and H_{ad} over the Pt(211) surface are given in Figure 10a−d. The binding energy for H on the Pt(211) step is about 3 eV, similar to that reported by Olsen et al.,[51] and nearly 0.2 eV stronger than on the (111) terrace, as seen for both Pt(211)[51] and Cu(211).[52] In addition, the CH_xO adsorbates also bind more strongly at the step sites (Table 1). This is expected considering the higher d-band positions of the metal atoms and the lower coordination number at these sites.[53]

Reaction energies for initial C−H and O−H cleavage over Pt(111) have been reported in the literature to be −0.16 and +0.62 eV, respectively, by Greeley et al.,[45,46] and −0.17 and +0.66 eV, respectively, by Desai et al.[44] The calculations performed herein over Pt(111) [i.e., (3 × 3) unit cell, 3 layers Pt] give C−H and O−H dehydrogenation energies of −0.33 and +0.66 eV, respectively (Table 1). The corresponding reaction energies for the C−H and O−H cleavage steps over the Pt(211) surface are calculated to be more favorable at −0.60 and −0.17 eV, respectively (Table 1). The overall activation of both bonds appears to be more favorable over the stepped surface, due to stronger binding of both the CH_2OH_{ad} (or CH_3O_{ad}) and the H_{ad} product species. However, the enhanced binding of the CH_3O at the Pt(211) step (by 0.74 eV) as compared to CH_2OH (by 0.2 eV, similar to H) results in O−H cleavage that becomes increasingly more competitive with that for C−H cleavage as compared to reactions over the (111) surface. This indicates that the role of surface defects can

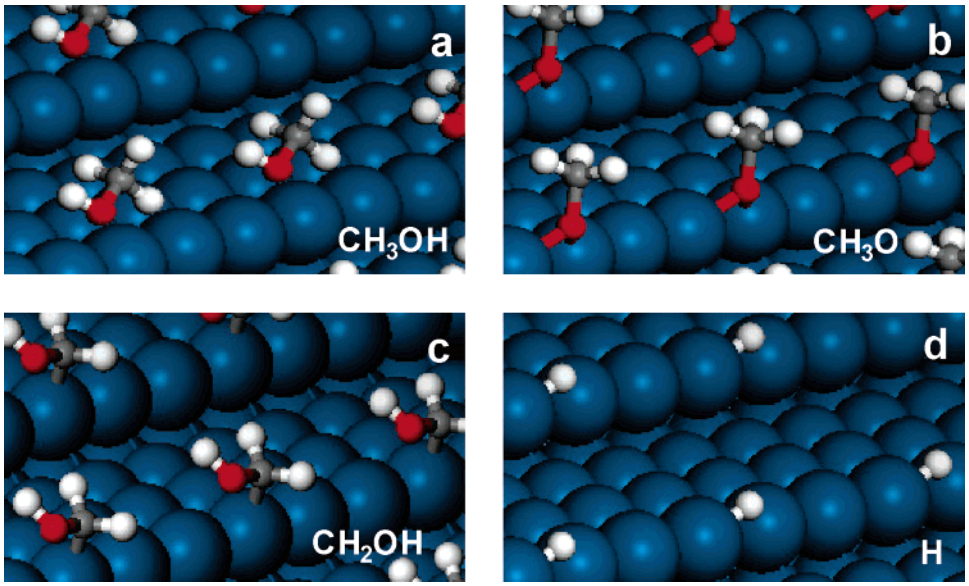

Figure 10. Optimized structures and binding sites of CH_3OH, CH_3O, CH_2OH, and H, as indicated, on the Pt(211) surface as determined by DFT.

significantly influence the reaction mechanism. Assuming that differences in the potential-dependent behavior of the aqueous-phase reaction energies loosely track the differences in the vapor-phase reaction energies for the (111) and (211) surfaces, it is quite likely that O−H cleavage at an exposed step edge would become equally and perhaps more favorable to corresponding C−H cleavage at moderately positive potentials in agreement with the experimental potential-dependent variation in *r*. It should once again be pointed out that we have only considered here the overall reaction energies. A more complete analysis would require the calculation of activation barriers.

The lack of direct agreement between the onset potential of the dual path over Pt(111) from experimental CA/CV results (+0.35 V vs RHE) and the trends predicted from the quantum-mechanical calculations demonstrate the difficulty in modeling the complexity of the electrocatalytic system. As discussed in ref 26, the method utilized here for determining the surface potential and corresponding potential-dependent reaction energetics from quantum-mechanical calculations utilizes assumptions of the structure of the solvent layer, the capacitance of the upper and lower slab surfaces, as well as the magnitude of the vacuum potential on the hydrogen scale.[28,29] Additionally, our analysis determines the mechanistic behavior from thermodynamic quantities using the Bell−Evans−Polanyi approach, yet disregards any kinetic limitations. Therefore, the calculational results should be taken as an indicator of the potential-dependence of the dual path and not be quantitatively compared to the experimental measurement.

5. Conclusions

The above analysis represents a combined experimental and quantum-mechanical approach to elucidating surface structure-dependent and potential-dependent differences in the dehydrogenation pathway of methanol over low Miller index planes of platinum single-crystal electrode surfaces. Experimental elucidation involves determining the ratio (*r*) of the integrated charge from subsequent chronoamperometry and fast-scan cyclic voltammetry steps, where *r* values less than 2 indicate full dehydrogenation to form stable CO_{ad} and *r* values greater than 2 indicate the presence of a dual path where incomplete dehydrogenation occurs in addition to forming CO_{ad}. In general, methanol oxidation over Pt(111) and (110) surfaces appears to occur via full dehydrogenation to form stable CO_{ad} surface species at potentials less than +0.35 V vs RHE and via a second incomplete dehydrogenation pathway toward higher potentials, whereas over the (100) surface, the reaction forms CO_{ad} only over a wide potential range.

For the (111) surface, full potential-dependent aqueous-phase periodic DFT calculations also indicate the presence of the dual path toward more positive potentials in addition to giving insight into the elementary steps of the methanol dehydrogenation pathway. The calculations indicate that the path to form stable CO_{ad} occurs via an initial exothermic C−H cleavage step to form adsorbed hydroxymethyl over a wide potential range, followed by exothermic dehydrogenation steps to form CO_{ad}. The pathway for incomplete dehydrogenation, however, is predicted to occur via an initial O−H cleavage step to form adsorbed methoxy (which is expected to be competitive to C−H cleavage at quite positive potentials) followed by exothermic C−H cleavage to form adsorbed formaldehyde (which can subsequently desorb into solution), indicating that the dehydrogenation product formed in the chronoamperometry experiments may be formaldehyde. Preliminary results for the inital C−H and O−H cleavage steps over a stepped Pt(211) surface indicate the prevalence for the parallel path toward positive potentials may be due to preferred initial O−H cleavage over defect sites. This combined experimental and quantum-mechanical approach provides an example of how such complementary methods can be utilized to help elucidate fundamental aspects of reaction chemistry at a molecular level.

Acknowledgment. We gratefully acknowledge the Army Research Office for funding through a MURI grant (DAAD19-03-1-0169) for fuel-cell research to Case Western Reserve University and the Environmental Molecular Sciences Laboratory at Pacific Northwest National Lab for computational resources. M.N. and S.A.W. would also like to thank Professor Jean-Sebastian Filhol and Christopher Taylor for their invaluable discussions.

References and Notes

(1) Parsons, R.; Vandernoot, T. *J. Electroanal. Chem.* **1988**, *257*, 9−45.
(2) Jarvi, T. D.; Stuve, E. M. In *Electrocatalysis*; Lipkowski, J., Ross, P. N., Eds.; Wiley−VCH: New York, 1998; pp 75−153.
(3) Hamnett, A. In *Interfacial Electrochemistry*; Wieckowski, A., Ed.; Marcel Dekker: New York, 1999; pp 843−883.
(4) Markovic, N. M.; Ross, P. N. *Surf. Sci. Rep.* **2002**, *45*, 121−229.
(5) Iwasita, T. *Electrochim. Acta* **2002**, *47*, 3663−3674.
(6) Herrero, E.; Franaszczuk, K.; Wieckowski, A. *J. Phys. Chem.* **1994**, *98*, 5074−5083.
(7) Chen, Y. X.; Miki, A.; Ye, S.; Sakai, H.; Osawa, M. *J. Am. Chem. Soc.* **2003**, *125*, 3680−3681.
(8) Childers, C. L.; Huang, H. L.; Korzeniewski, C. *Langmuir* **1999**, *15*, 786−789.
(9) Korzeniewski, C.; Childers, C. L. *J. Phys. Chem. B* **1998**, *102*, 489−492.
(10) Batista, E. A.; Malpass, G. R. P.; Motheo, A. J.; Iwasita, T. *Electrochem. Commun.* **2003**, *5*, 843−846.
(11) Wang, H. S.; Wingender, C.; Baltruschat, H.; Lopez, M.; Reetz, M. T. *J. Electroanal. Chem.* **2001**, *509*, 163−169.
(12) Wang, H.; Loffler, T.; Baltruschat, H. *J. Appl. Electrochem.* **2001**, *31*, 759−765.
(13) Ota, K.-I.; Nakagawa, Y.; Takahashi, M. *J. Electroanal. Chem.* **1984**, *179*, 179−186.
(14) Xia, X. H.; Iwasita, T.; Ge, F.; Vielstich, W. *Electrochim. Acta* **1996**, *41*, 711−718.
(15) Iwasita, T.; Nart, F. C.; Lopez, B.; Vielstich, W. *Electrochim. Acta* **1992**, *37*, 2361−2367.
(16) Lopes, M. I. S.; Beden, B.; Hahn, F.; Leger, J. M.; Lamy, C. *J. Electroanal. Chem.* **1991**, *313*, 323−339.
(17) Papoutsis, A.; Leger, J. M.; Lamy, C. *J. Electroanal. Chem.* **1987**, *234*, 315−327.
(18) Lu, G. Q.; Chrzanowski, W.; Wieckowski, A. *J. Phys. Chem. B* **2000**, *104*, 5566−5572.
(19) Herrero, E.; Chrzanowski, W.; Wieckowski, A. *J. Phys. Chem.* **1995**, *99*, 10423−10424.
(20) Sriramulu, S.; Jarvi, T. D.; Stuve, E. M. *J. Electroanal. Chem.* **1999**, *467*, 132−142.
(21) Sriramulu, S.; Jarvi, T. D.; Stuve, E. M. *Electrochim. Acta* **1998**, *44*, 1127−1134.
(22) Jarvi, T. D.; Sriramulu, S.; Stuve, E. M. *J. Phys. Chem. B* **1997**, *101*, 3649−3652.
(23) Tremiliosi, G.; Kim, H.; Chrzanowski, W.; Wieckowski, A.; Grzybowska, B.; Kulesza, P. *J. Electroanal. Chem.* **1999**, *467*, 143−156.
(24) Clavilier, J. In *Interfacial Electrochemistry*; Wieckowski, A., Ed.; Marcel Dekker: New York, 1999; pp 231−248.
(25) Kibler, L. A.; Cuesta, A.; Kleinert, M.; Kolb, D. M. *J. Electroanal. Chem.* **2000**, *484*, 73−82.
(26) Taylor, C.; Wasileski, S. A.; Fanjoy, J.; Filhol, J. S.; Neurock, M., in preparation.
(27) The vacuum potential at the position bisecting the upper and lower slabs is converged for vacuum-layer thicknesses greater than 15 Å.
(28) Wagner, F. T. In *Structure of Electrofied Interfaces*; Lipkowski, J., Ross, P. N., Eds.; VCH Publishers: New York, 1993; Chapter 9.
(29) Trasati, S. *Electrochim. Acta* **1991**, *36*, 1657.
(30) Taylor, C.; Kelly, R.; Neurock, M., to be published.
(31) Housmanns, T. H. M.; Koper, M. T. M. *J. Phys. Chem. B* **2003**, *107*, 8557.
(32) *Vienna Ab initio Simulation Package (VASP), VASP 4.6*; Institute for Materialphysics, University of Vienna: Vienna, Austria, 2003.
(33) Perdew, J. P.; Burke, K.; Ernzerhof, M. *Phys. Rev. Lett.* **1996**, *77*.

(34) Perdew, J. P.; Burke, K.; Ernzerhof, M. *Phys. Rev. Lett.* **1998**, *80*, 891.

(35) Perdew, J. P.; Chevary, J. A.; Vosko, S. H.; Jackson, K. A.; Pederson, M. R.; Singh, D. J.; Fiolhais, C. *Phys. Rev. B* **1992**, *46*, 6671.

(36) Vanderbilt, D. *Phys. Rev. B* **1990**, *41*, 7892.

(37) Hammer, B.; Hansen, L. B.; Nørskov, J. K. *Phys. Rev. B* **1999**, *59*, 7413.

(38) Monkhorst, H. J.; Pack, J. D. *Phys. Rev. B* **1976**, *13*, 5188.

(39) Methfessel, M.; Paxton, A. T. *Phys. Rev. B* **1989**, *40*, 3616.

(40) The procedure for combined chronoamperometry and fast scan cyclic voltammetry experiments applied to each type of platinum surfaces was slightly different and was optimized accordingly. The cleaning steps for Pt(110) are the same as those for Pt(111). Cyclic voltammetry was performed at 20 V/s between 0.02 and 1.0 V. The cleaning steps for Pt(100) were 0.55 V (1 s) → 1.0 V (1 s) → 0.01 V (1 s) → 1.0 V (1 s) → 0.01 V (1 s) → 1.0 V (1 s) → 0.175 V (0.5 s) → E_M. Cyclic voltammograms were recorded at 20 V/s between 0.06 and 1.05 V.

(41) Gamboaaldeco, M. E.; Herrero, E.; Zelenay, P. S.; Wieckowski, A. *J. Electroanal. Chem.* **1993**, *348*, 451.

(42) Kua, J.; Goddard, W. A. *J. Am. Chem. Soc.* **1999**, *121*, 10928.

(43) Ishikawa, Y.; Liao, M.-S.; Cabrera, C. R. *Surf. Sci.* **2000**, *463*, 66.

(44) Desai, S. K.; Neurock, M.; Kourtakis, K. *J. Phys. Chem. B* **2002**, *106*, 2559.

(45) Greeley, J.; Mavrikakis, M. *J. Am. Chem. Soc.* **2002**, *124*, 7193.

(46) Greeley, J.; Mavrikakis, M. *J. Am. Chem. Soc.* **2004**, *126*, 3910.

(47) Okamoto, Y.; Sugino, O.; Mochizuki, Y.; Ikeshoji, T.; Morikawa, Y. *Chem. Phys. Lett.* **2003**, *377*, 236.

(48) Mattsson, T.; Paddison, S. *Surf. Sci. Lett.* **2003**, *544*, L697.

(49) Neurock, M.; Wasileski, S. A.; Mei, D. *Chem. Eng. Sci.* **2004**, *59*, 4703.

(50) Filhol, J. S.; Neurock, M., to be published.

(51) Olsen, R. A.; Badescu, S. C.; Ying, S. C.; Baerends, E. J. *J. Chem. Phys.* **2004**, *120*, 11852.

(52) Sljivancanin, Z.; Hammer, B. *Phys. Rev. B* **2002**, *65*, 085414.

(53) Hammer, B. *Surf. Sci.* **2000**, *459*, 323.